A sysytem of alternately exited coupled non-autonomous oscillators manifesting phenomena intrinsic to complex analytic maps

Olga B. Isaeva[a*], Sergey P. Kuznetsov[a]
and
Andrew H. Osbaldestin[b]

[a] *Kotel'nikov Institute of Radio-Engineering and Electronics of RAS, Saratov Branch Zelenaya 38, Saratov, 410019, Russian Federation*

[b] *Department of Mathematics, University of Portsmouth, Portsmouth, PO1 3HE, UK*

*IsaevaO@rambler.ru

Abstract

A feasible model is introduced that manifests phenomena intrinsic to iterative complex analytic maps (like Mandelbrot set, Julia sets etc.). The system is composed of two coupled alternately excited oscillators. The idea is based on a turn-by-turn transfer of the excitation from one subsystem to another (S.P. Kuznetsov, Phys. Rev. Lett. **95** , 2005, 144101) accompanied with appropriate nonlinear transformation of the complex amplitude of the oscillations in the course of the process. Analytic and numerical studies are performed. Special attention is paid to analysis of violation of the applicability of the slow amplitude method with decrease of the ratio of a period of the excitation transfer to a basic period of the oscillations. The main effect consists in rotation of the Mandelbrot-like set in the complex parameter plane; one more effect is destruction of subtle small-scale fractal structure of the set due to presence of non-analytic terms in the complex amplitude equations.

*PACS:*05.45.-a

*Keywords:*Mandelbrot and Julia sets; complex analytic maps; coupled oscillators.

1 Introduction

One special chapter of nonlinear dynamics elaborated extensively by mathematicians consists in a study of iterative maps defined by analytic functions of complex variable. A classic object is a complex quadratic map [1]

$$z_{n+1} = c + z_n^2. \tag{1}$$

At $c = 0$ the behavior of the iterations is rather evident: for $|z_0| > 1$ the result diverges to infinity, and for $|z_0| < 1$ one observes residence of the variable z in a bounded part of the complex plane.

The border between these two kinds of behavior is a unit circle $|z_0| = 1$. At other values of the complex parameter c a set on the complex plane z, separating the analogous two types of behavior appears to be rather complicated and nontrivial (fractal). It is called a Julia set (see examples in Fig. 1).

Alternatively, we can fix the initial condition $z_0 = 0$ and consider behavior of the iterations in dependence on the complex parameter c. Then, at some values of c the iterations escape to infinity, and at others they stay in a bounded domain. A set on the complex plane c associated with this last situation is called the Mandelbrot set (see Fig. 1a). Note that the bounded dynamics may be periodic or chaotic. The domain of periodic behavior resembles a cactus and consists of a set of roundish formations touching each other and placed around one big area in a form of a cardioid. Figures 1, 2, 3 on the plot designate periods of dynamics observed in several basic leaves of the "cactus". Chaotic dynamics takes place at points corresponding to the fractal pattern setting off the "cactus". The dots in Fig. 1a indicate parameter values, for which the Julia sets are shown in panels (b-f).

A challenging problem is realization of the phenomena intrinsic to the complex analytic maps in physical systems (see, e.g. [2]). One successful attempt to implement this dynamics relates to a symmetric system of coupled maps for two real variables or to a system of two periodically driven coupled nonlinear oscillators [3]. In this context an interpretation of the Mandelbrot set was suggested, as a domain of generalized partial synchronization [4], and some aspects of feasibility of the phenomena of complex dynamics in autonomous flow systems were studied [5]. An electronic analog device was designed simulating the dynamics of two coupled quadratic maps, in which the Mandelbrot-like set was observed for the first time in a physical experiment [6].

In the present paper, we suggest an alternative approach that gives an opportunity to organize dynamics similar to that in the complex analytic maps. The main idea is based on interpretation of a complex amplitude of an oscillatory process as a complex variable. Two alternately excited oscillators are used to pass the excitation each other with transformation of the complex amplitude corresponding approximately to the complex quadratic map. Earlier a similar idea was applied to construct physical systems delivering realistic examples for some well-known abstract concepts and phenomena of the nonlinear science, like Bernoulli map, Smale - Williams attractor, Arnold's cat map, robust strange nonchaotic attractor [7, 8, 9, 10, 11].

In Sec. 2 we introduce a system of coupled oscillators alternately activated by means of modulation of the dissipation parameter accompanied with a turn-by-turn transfer of the excitation between the subsystems. In Sec. 3 we derive the shortened equations for the system using the complex amplitude approach. Then, we undertake an approximate analytic solution of the equations. The result is the complex quadratic mapping, which represents the Poincaré map for the system and governs the state evolution on one period of the parameter modulation. We present and compare pictures on the parameter plane and the phase space portraits for the amplitude equations and those for the approximate analytic map (the Mandelbrot set and the Julia sets). In Sec. 4 we turn again to the original coupled oscillator equations and consider results of numerical studies to observe and discuss deviations from the slow-amplitude approach, which become relevant with decrease of a parameter N representing a ratio of the modulation period to the basic period of oscillations. We find that the most notable effect consists in rotation of the Mandelbrot-like set in the complex parameter plane while its visible fractal-like structure persists. In addition, we reveal gradual destruction of subtle details of this fractal structure (starting from smaller scales) as the

parameter N departs from the range of applicability of the method of slow amplitudes. We relate this phenomenon to non-resonance complex conjugate terms in the equations of the oscillators (rewritten in terms of the complex variables), which are negligible in the large N asymptotics.

2 The basic model system and its operation

In the oscillation and wave theory, a method of slow amplitudes is known. An oscillatory process possessing a basic frequency ω_0 is attributed with slow complex amplitude $A(t)$ as follows: $x(t) = A(t)e^{i\omega_0 t} + A^*(t)e^{-i\omega_0 t} = 2\mathrm{Re}[A(t)e^{i\omega_0 t}]$, where asterisk designates a complex conjugate. Transformation of this signal by means of a quadratic nonlinearity yields $y(t) = [x(t)]^2 = 2|A(t)|^2 + 2\mathrm{Re}\{[A(t)]^2 e^{2i\omega_0 t}\}$. As seen, the doubled frequency component has the complex amplitude equal to the squared complex amplitude of the original signal. Such a transformation will be a main element of the approach we develop to realization of phenomena of complex analytic dynamics.

Let us consider a system of two coupled non-autonomous oscillators

$$\begin{gathered} \ddot{x} + \omega_0^2 x + F \cdot (\gamma + \sin \Omega t)\dot{x} = \varepsilon y \sin \omega_0 t + \lambda \sin(\omega_0 t + \varphi), \\ \ddot{y} + (2\omega_0)^2 y + F \cdot (\gamma - \sin \Omega t)\dot{y} = \varepsilon x^2, \end{gathered} \tag{2}$$

where x and y represent generalized coordinates for the first and the second oscillator, respectively, and F, γ, λ, φ, ε are parameters. The first oscillator has a characteristic frequency ω_0, and the second one has a frequency twice as large. Parameters controlling dissipation in the both oscillators vary in counter-phase slowly. The period of modulation $T = 2\pi/\Omega$ is assumed equal to an integer number N of periods of basic oscillations $2\pi/\omega_0$.

One can describe the dynamics in terms of discrete time by means of the Poincaré map. Been given a vector $\mathbf{x}_n = \{x(t_n), u(t_n), y(t_n), v(t_n)\} = \{x(t_n), \dot{x}(t_n)/\omega_0, y(t_n), \dot{y}(t_n)/2\omega_0\}$ as a state of the system at $t_n = nT + t_0$, from solution of the differential equations (2) with the initial condition $\mathbf{x}_n$, we get a new vector $\mathbf{x}_{n+1}$ at $t_{n+1} = (n+1)T + t_0$. As it is determined uniquely by $\mathbf{x}_n$, we may introduce a function that maps the four-dimensional space $\{x, u, y, v\}$ into itself: $\mathbf{x}_{n+1} = \mathbf{T}(\mathbf{x}_n)$. This Poincaré map appears due to evolution determined by the differential equations with smooth and bounded right-hand parts in a finite domain of variables $\{x, u, y, v\}$. In accordance with theorems of existence, uniqueness, continuity, and differentiability of solutions of differential equations, the map $\mathbf{T}$ is a diffeomorphism, a one-to-one differentiable map of class $\mathbb{C}^\infty$.

Let us consider qualitatively how does the system (2) operate. The constant γ is supposed to be positive, less than 1. Been in average positive, on a certain part of the modulation period the dissipation parameter $F(\gamma + \sin \Omega t)$ for each oscillator becomes negative. On that interval, the oscillator is active (the oscillations grow). On the rest part of the modulation period, it is passive (the oscillations decay). Let us assume that at the beginning of the active stage of the second oscillator, the first one oscillates with complex amplitude A: $x(t) \propto \mathrm{Re}(Ae^{i\omega_0 t})$. Then, the "germ" for excitation of the second oscillator (see the right-hand part of the second equation) is the second harmonic component produced by the nonlinear quadratic transformation of the signal from the first oscillator, $\mathrm{Re}(A^2 e^{2i\omega_0 t})$. As follows, the complex amplitude of the second oscillator on its active stage will be proportional to A^2. Mixing with the auxiliary signal (see the right-hand part of the first equation) gives rise to a difference frequency component ω_0 with amplitude proportional to A^2. Then, a sum of this component with an additional oscillatory

term of frequency ω_0, amplitude λ and phase φ, produces a "germ" for the excitation of the first oscillator. Its complex amplitude is proportional to A^2 plus a complex constant. Hence, the stroboscopic Poincaré map reduced in a certain approximation to two-dimensional map and expressed in terms of complex amplitudes corresponds to the complex quadratic map. The role of complex parameter belongs to the number of modulus λ and argument φ. In dependence on this parameter and initial conditions, it may happen that the solution for the equations of coupled non-autonomous oscillators either is bounded or escapes to infinity. A domain on the complex parameter plane $\lambda e^{i\varphi}$, where bounded attractors persist, will be analog of the Mandelbrot set. Sets in the phase space separating initial conditions of bounded and unbounded motions will be analogs of the Julia sets.

3 Amplitude equations, slow-amplitude asymptotics and derivation of an approximate Poincaré map

To derive equations for complex amplitudes in the system of two coupled oscillators we set

$$x = Ae^{i\omega_0 t} + A^* e^{-i\omega_0 t}, \qquad y = Be^{2i\omega_0 t} + B^* e^{-2i\omega_0 t} \tag{3}$$

with additional conditions

$$\dot{A}e^{i\omega_0 t} + \dot{A}^* e^{-i\omega_0 t} = 0, \qquad \dot{B}e^{2i\omega_0 t} + \dot{B}^* e^{-2i\omega_0 t} = 0. \tag{4}$$

Substitution into the equations (2) yields

$$\begin{aligned} 2i\omega_0 \dot{A}e^{i\omega_0 t} + i\omega_0 (Ae^{i\omega_0 t} - A^* e^{-i\omega_0 t}) F(\gamma + \sin\Omega t) = \\ \varepsilon (Be^{2i\omega_0 t} + B^* e^{-2i\omega_0 t}) \sin\omega_0 t + \lambda \sin(\omega_0 t + \varphi), \\ 4i\omega_0 \dot{B}e^{2i\omega_0 t} + 2i\omega_0 (Be^{2i\omega_0 t} - B^* e^{-2i\omega_0 t}) F(\gamma - \sin\Omega t) = \varepsilon (Ae^{i\omega_0 t} + A^* e^{-i\omega_0 t})^2, \end{aligned} \tag{5}$$

or, after multiplication of the first and the second equations by $(2i\omega_0 e^{i\omega_0 t})^{-1}$ and $(4i\omega_0 e^{2i\omega_0 t})^{-1}$, respectively,

$$\begin{aligned} \dot{A} + (F/2)(\gamma + \sin\Omega t)(A - A^* e^{-2i\omega_0 t}) = \\ -(\varepsilon/2\omega_0)(Be^{2i\omega_0 t} + B^* e^{-2i\omega_0 t})(1 - e^{-2i\omega_0 t}) - (\lambda/2\omega_0)(e^{i\varphi} - e^{-2i\omega_0 t - i\varphi}), \\ \dot{B} + (F/2)(\gamma - \sin\Omega t)(B - B^* e^{-4i\omega_0 t}) = (\varepsilon/4i\omega_0)(A + A^* e^{-2i\omega_0 t})^2. \end{aligned} \tag{6}$$

The relations (6) are equivalent to the original equations (2) completely, although written in terms of the complex amplitudes A and B.

An approximation used widely in the oscillation and wave theory consists in assumption that variation of the amplitudes A and B in time is slow, and one can neglect the fast oscillating terms in (6). Formally, they are excluded by means of averaging the equations over a period $2\pi\omega_0^{-1}$. This approximation is justified in the case of a large frequency ratio $N = \omega_0/\Omega >> 1$. In this way, we arrive at the shortened slow-amplitude equations

$$\begin{aligned} \dot{A} + (F/2)(\gamma + \sin\Omega t)A = \varepsilon B/(4\omega_0) - \lambda e^{i\varphi}/(4\omega_0), \\ \dot{B} + (F/2)(\gamma - \sin\Omega t)B = \varepsilon A^2/(4i\omega_0). \end{aligned} \tag{7}$$

With some additional assumptions, it is possible to construct analytically an approximate Poincaré map for these equations.

Let us start with consideration of a subsidiary differential equation

$$\dot{w} + g'(t)w = K(t)e^{f(t)}, \tag{8}$$

where g and f are some smooth real-value functions. We represent a solution as

$$w(t) = C(t)e^{-g(t)}, \tag{9}$$

assuming the time-dependent coefficient $C(t)$ to satisfy

$$\dot{C} = K(t)e^{f(t)+g(t)}. \tag{10}$$

Consider a time interval containing a single maximum of the function $f(t) + g(t)$ at $t = t_0$:

$$f'(t_0) + g'(t_0) = 0, \qquad f''(t_0) + g''(t_0) = -\beta < 0. \tag{11}$$

Integral of the equation (10) over the time interval can be evaluated with a help of the Laplace method. It yields

$$\int K(t)e^{f(t)+g(t)}\,dt \approx K(t_0)e^{f(t_0)+g(t_0)} \int e^{-\beta t^2/2}\,dt = K(t_0)e^{f(t_0)+g(t_0)}\sqrt{2\pi/\beta}. \tag{12}$$

Let the solution (9) be zero to the left side from the maximum, then

$$C(t) = \begin{cases} 0,\ t < t_0 - h, \\ K(t_0)\sqrt{2\pi/\beta}e^{f(t_0)+g(t_0)},\ t > t_0 + h, \end{cases} \tag{13}$$

and

$$w(t) = \begin{cases} 0,\ t < t_0 - h, \\ K(t_0)\sqrt{2\pi/\beta}e^{f(t_0)+g(t_0)}e^{-g(t)},\ t > t_0 + h. \end{cases} \tag{14}$$

Here h may be thought as a characteristic width of the "hump" of the function $f + g$.

Now we return to the amplitude equations (7). Let us consider separately two parts of one period of modulation.

The first is a part containing a time interval of activity of the first oscillator; its amplitude is there relatively large, while the second oscillator is passive and possesses very small amplitude. Here we may account only effect of the first oscillator on the second one and neglect the backward coupling, i.e. regard the coupling as unidirectional.

Excluding the right-hand part of the first equation, we write down for the slow amplitude of the first oscillator

$$A(t) = C_A \exp\left[-\frac{F}{2}(\gamma t - \Omega^{-1}\cos\Omega t)\right]. \tag{15}$$

Let us define the value t_n as associated with a maximum of $|A|$. It satisfies the relations

$$\sin\Omega t_n = -\gamma, \qquad \cos\Omega t_n = \sqrt{1-\gamma^2} > 0. \tag{16}$$

Resolving (16) in respect to t_n, substitute it into (15) and designate $A_n = A(t_n)$. Then,

$$C_A = A_n \exp\left[-\frac{F}{2\Omega}\left(\gamma \arctan\frac{\gamma}{\sqrt{1-\gamma^2}} + \sqrt{1-\gamma^2}\right)\right]. \tag{17}$$

For the second oscillator we write down

$$\dot{B} + \frac{F}{2}(\gamma - \sin\Omega t)B = \frac{\varepsilon}{4i\omega_0}C_A^2 \exp\left[-F(\gamma t - \Omega^{-1}\cos\Omega t)\right]. \tag{18}$$

To solve this equation we use the result (14) obtained for the subsidiary problem (8). To do this, we have to set

$$\begin{gathered} g'_{A\to B}(t) = (F/2)(\gamma - \sin\Omega t), \qquad f_{A\to B}(t) = -F(\gamma t - \Omega^{-1}\cos\Omega t), \\ K_{A\to B} = [\varepsilon/(4i\omega_0)]C_A^2 \end{gathered} \tag{19}$$

and

$$\begin{gathered} g_{A\to B}(t) + f_{A\to B}(t) = -(1/2)F\gamma t + (3/2)F\Omega^{-1}\cos\Omega t, \\ g'_{A\to B}(t) + f'_{A\to B}(t) = -(1/2)F\gamma - (3/2)F\sin\Omega t, \\ g''_{A\to B}(t) + f''_{A\to B}(t) = -(3/2)F\Omega\cos\Omega t. \end{gathered} \tag{20}$$

From a condition of vanishing the first derivative and a requirement for the second derivative to be negative, we determine the time instant $t_{A\to B}$, neighborhood of which corresponds to the excitation of the second oscillator by the first one. It satisfies

$$\sin\Omega t_{A\to B} = -\gamma/3, \qquad \cos\Omega t_{A\to B} = \sqrt{1-\gamma^2/9}. \tag{21}$$

Here

$$g''_{A\to B}(t_{A\to B}) + f''_{A\to B}(t_{A\to B}) = -\beta_{A\to B} = -(3/2)F\Omega\cos\Omega t_{A\to B} = -(3/2)F\Omega\sqrt{1-\gamma^2/9}. \tag{22}$$

Applying the formula (14), we obtain the asymptotic solution for the amplitude B

$$B(t) = \begin{cases} 0,\ t < t_{A\to B} - h, \\ C_B \exp\left[-\frac{F}{2}(\gamma t + \Omega^{-1}\cos\Omega t)\right],\ t > t_{A\to B} + h, \end{cases} \tag{23}$$

where

$$C_B = \frac{\varepsilon C_A^2}{4i\omega_0}\sqrt{\frac{2\pi}{(3/2)F\Omega\sqrt{1-\gamma^2/9}}}e^{g_{A\to B}(t_{A\to B}) + f_{A\to B}(t_{A\to B})}. \tag{24}$$

On the second part of the modulation period, which we start to consider now, the amplitude of the second oscillator is relatively large, and that of the first oscillator is small. Here we may again regard the coupling as unidirectional and account only effect of the second oscillator on the first one. For the first oscillator we write down

$$\dot{A} + \frac{F}{2}(\gamma + \sin\Omega t)A = \frac{\varepsilon}{4\omega_0}C_B \exp\left[-\frac{F}{2}(\gamma t + \Omega^{-1}\cos\Omega t)\right] - \frac{1}{4\omega_0}\lambda e^{i\varphi}. \tag{25}$$

The right-hand part contains two terms. Accounting linearity of the equation, we will obtain solution as a superposition of two components corresponding to separate contribution of these terms: $A(t) = A_{B\to A}(t) + A_\lambda(t)$.

Let us consider first the solution $A_{B\to A}(t)$ accounting driving by the second oscillator. Again, we may exploit the result for the subsidiary equation setting

$$\begin{gathered} g'_{B\to A}(t) = (F/2)(\gamma + \sin\Omega t), \qquad f_{B\to A}(t) = -(F/2)(\gamma t + \Omega^{-1}\cos\Omega t), \\ K_{B\to A} = [\varepsilon/(4\omega_0)]C_B \end{gathered} \tag{26}$$

and

$$\begin{gathered} g_{B\to A}(t)+f_{B\to A}(t)=-F\Omega^{-1}\cos\Omega t,\\ g'_{B\to A}(t)+f'_{B\to A}(t)=F\sin\Omega t,\\ g''_{B\to A}(t)+f''_{B\to A}(t)=F\Omega\cos\Omega t. \end{gathered} \tag{27}$$

From the condition of maximum for the function $g_{B\to A}+f_{B\to A}$

$$\sin\Omega t_{B\to A}=0,\qquad \cos\Omega t_{B\to A}=-1 \tag{28}$$

we determine a time instant $t_{B\to A}$, neighborhood of which is responsible for excitation of the first oscillator. With application of the formula (14) and accounting the relation

$$g''_{B\to A}(t_{B\to A})+f''_{B\to A}(t_{B\to A})=-\beta_{B\to A}=-F\Omega \tag{29}$$

we obtain

$$A_{B\to A}(t)=\begin{cases} 0,\ t<t_{B\to A}-h,\\ \frac{\varepsilon}{4\omega_0}C_B\sqrt{\frac{2\pi}{F\Omega}}e^{F/\Omega}\exp\left[-\frac{F}{2}(\gamma t-\Omega^{-1}\cos\Omega t)\right],\ t>t_{B\to A}+h. \end{cases} \tag{30}$$

Let us turn now to a solution A_λ associated with the second term in the right-hand part of the equation (25). Now we set

$$g'_\lambda(t)=(F/2)(\gamma+\sin\Omega t),\qquad f_\lambda(t)=0,\qquad K_\lambda=-[1/(4\omega_0)]\lambda e^{i\varphi} \tag{31}$$

and

$$\begin{gathered} g_\lambda(t)+f_\lambda(t)=(1/2)F\gamma t-(1/2)F\Omega^{-1}\cos\Omega t,\\ g'_\lambda(t)+f'_\lambda(t)=(1/2)F\gamma+(1/2)F\sin\Omega t,\\ g''_\lambda(t)+f''_\lambda(t)=(1/2)F\Omega\cos\Omega t. \end{gathered} \tag{32}$$

Then, we determine t_λ corresponding to maximum of the function $g_\lambda+f_\lambda$

$$\sin\Omega t_\lambda=-\gamma,\qquad \cos\Omega t_\lambda=-\sqrt{1-\gamma^2}. \tag{33}$$

Then

$$g''_\lambda(t_\lambda)+f''_\lambda(t_\lambda)=-\beta_\lambda=-(1/2)F\Omega\sqrt{1-\gamma^2} \tag{34}$$

and, in accordance with the formula (14),

$$A_\lambda(t)=\begin{cases} 0,\ t<t_\lambda-h,\\ \frac{\lambda e^{i\varphi}}{4\omega_0}\sqrt{\frac{4\pi}{F\Omega\sqrt{1-\gamma^2}}}e^{g_\lambda(t_\lambda)}\exp\left[-\frac{F}{2}(\gamma t-\Omega^{-1}\cos\Omega t)\right],\ t>t_\lambda+h. \end{cases} \tag{35}$$

Composing a sum of two solutions (30) and (35), for $t>\max(t_{B\to A},t_\lambda)$ we obtain

$$A(t)=\frac{1}{4\omega_0}\sqrt{\frac{2\pi}{F\Omega}}\left\{\varepsilon C_B e^{F/\Omega}-\lambda e^{i\varphi}\frac{\sqrt{2}}{\sqrt[4]{1-\gamma^2}}e^{g_\lambda(t_\lambda)}\right\}\exp\left[-\frac{F}{2}(\gamma t-\Omega^{-1}\cos\Omega t)\right]. \tag{36}$$

Finally, we evaluate the amplitude of the first oscillator at the end of the considered period $A_{n+1}=A(t_{n+1})=A(t_n+T)=A(t_n+2\pi/\Omega)$. With the relations (17), (20-21) and (32-33) it is expressed via the initial amplitude $A_n=A(t_n)$ as

$$\begin{gathered} A_{n+1}=\frac{\sqrt{\pi}}{2\omega_0\sqrt{F\Omega}\sqrt[4]{1-\gamma^2}}e^{\frac{F}{\Omega}\left(\gamma\arctan\frac{\gamma}{\sqrt{1-\gamma^2}}+\sqrt{1-\gamma^2}-\frac{\pi\gamma}{2}\right)}\times\\ \left\{A_n^2\frac{\varepsilon^2\sqrt{2\pi}\sqrt[4]{1-\gamma^2}}{4i\omega_0\sqrt{F\Omega}\sqrt{9-\gamma^2}}e^{\frac{F}{2\Omega}\left(\gamma\arctan\frac{\gamma}{\sqrt{9-\gamma^2}}-3\gamma\arctan\frac{\gamma}{\sqrt{1-\gamma^2}}+\sqrt{9-\gamma^2}-3\sqrt{1-\gamma^2}+2-\pi\gamma\right)}-\lambda e^{i\varphi}\right\}. \end{gathered} \tag{37}$$

By variable and parameter changes

$$z_n = -A_n \frac{i\sqrt{2}\pi\varepsilon^2}{8\omega_0^2 F\Omega \sqrt[4]{9-\gamma^2}} e^{\frac{F}{2\Omega}\left(\gamma \arctan\frac{\gamma}{\sqrt{9-\gamma^2}} - \gamma \arctan\frac{\gamma}{\sqrt{1-\gamma^2}} + \sqrt{9-\gamma^2} - \sqrt{1-\gamma^2} + 2 - 2\pi\gamma\right)}. \tag{38}$$

and

$$c = \lambda e^{i\varphi} \frac{i\sqrt{2}\varepsilon^2 [\pi/(F\Omega)]^{3/2}}{16\omega_0^3 \sqrt[4]{9-\gamma^2}\sqrt[4]{1-\gamma^2}} e^{\frac{F}{2\Omega}\left(\gamma \arctan\frac{\gamma}{\sqrt{9-\gamma^2}} + \gamma \arctan\frac{\gamma}{\sqrt{1-\gamma^2}} + \sqrt{9-\gamma^2} + \sqrt{1-\gamma^2} + 2 - 3\pi\gamma\right)} \tag{39}$$

the map (37) is reduced to the canonical form of the complex quadratic map (1).

In Fig. 2 we present diagrams obtained from computations for the map (37) and for the shortened amplitude equations (7) (see panels (a) and (b), respectively). Depicted is a plane of the complex parameter $\lambda e^{i\varphi}$; other parameters are $N = 10$, $F = 7$, $\gamma = 0.5$, $\varepsilon = 1$. Gray color corresponds to observation of dynamics with bounded amplitudes, and white to observed escape to infinity. The object on the diagram (b) for the set of differential equations (7) is evidently similar to the Mandelbrot cactus for the complex quadratic map (37). Marks 1, 2, 3,... on the diagrams indicate leaves, where the bounded dynamics of periods T, $2T$, $3T$, ... take place. Obviously, a type of regime is determined by the "germ" signal, which acts in the initial part of the active stage of the first oscillator been formed as a composition of the signal from the partner oscillator and of the external force. Essential are the phase relations of these two signals, which determine subtle structure of leaves of the "cactus" in the parameter plane.

At a certain point of the parameter plane $\lambda = 1.5i$ we present comparison of the time dependences for amplitudes of two oscillators obtained from numerical solution of the equation (7) (gray profiles) and those corresponding to the approximate analytic relations (15), (23), and (36) (dotted lines). Observe that the numerical and approximate analytic solutions manifest good agreement.

4 Numerical studies of the basic model system of coupled non-autonomous oscillators

Reduction of the dynamics to the complex quadratic map in the previous section was based on a use of the slow amplitude method (the large-N asymptotics) and of some additional approximations in the course of derivation of the analytic form of the Poincaré map.

Now we intend to return to the original system of coupled non-autonomous oscillators governed by the real-value equations (2). One may expect that at least in a "coarse" structure of the objects in the parameter plane and in the phase space will be similar to that of the Mandelbrot and Julia sets of the complex quadratic map. How well do subtler details of the structures correspond in the original system and in the reduced model, is an interesting and important question. In this section, we turn to results of numerical studies of the original system of coupled oscillators. As well, these results may be related to the equivalent set of equations rewritten in terms of the complex amplitudes without neglecting the oscillating terms (see (6).

In Fig. 3 we depict the Mandelbrot-like sets obtained from computations for the basic model (2). The grays are areas on the parameter plane corresponding to observation of periodic dynamics in a bounded domain of the dynamical variables. The most notable effect in comparison with the slow-amplitude approximation consists in a counter-clock-wise rotation of the pictures with a decrease

of N. Nevertheless, the visible structure of mutual disposition of "leaves" of the "cactuses" persists and corresponds to that intrinsic to the complex quadratic map (cf. Figs. 3 and 1). Hereafter, to avoid redundancy, we will speak of these objects as Mandelbrot cactuses for the coupled oscillator system (2).[1]

For detailed analysis, let us turn to a case of a relatively small N to observe notable deflections from the slow-amplitude asymptotic with a possibility of resolution of dissimilarity in the case of the basic model and that of the complex analytic map.

In Fig. 4 (panels a and b) we present pictures of the Mandelbrot cactus obtained in computations for the system of coupled non-autonomous oscillators at $N = 10$ and other parameters $\omega_0 = 2\pi$, $F = 7$, $\gamma = 0.5$, $\varepsilon = 1$. Except the approximately right angle turn, the object looks similar to those for the complex map and for the shortened amplitude equations (see Figs. 2a, b). For parameter values marked with dots on the picture of the cactus, we depict diagrams on the plane of variables of the first oscillator $(x, \dot{x}/\omega_0)$, which are analogous to portraits of Julia sets for the complex quadratic map in Fig. 1. To be accurate, we have to note that in the system of coupled oscillators we deal with a four-dimensional phase space $(x, \dot{x}/\omega_0, y, \dot{y}/2\omega_0)$. In the stroboscopic Poincaré map (as it defined in Section 2), attractor is placed close to the coordinate plane $(x, \dot{x}/\omega_0)$, but not precisely in it. The basin of attraction is naturally a four-dimensional object. Diagrams in panels (g-j) of Fig. 4 correspond to cross-sections of those four-dimensional basins by the plane $y = 0$, $\dot{y} = 0$ for the attractors belonging to a bounded region of the phase space. Portraits of respective attractors in projection onto the plane are shown on panels (c-f). Dots inside the basins correspond to stroboscopic cross-sections for the attractive periodic orbits. Figure 5 illustrates dynamics of the system on an attractive orbit of period $3T$ for the parameter value $\lambda e^{i\varphi} = -0.2 + 1.5i$ (it is located inside the "leave" of the cactus shown with magnification in Fig. 4 b).

As seen from the presented material, our model system indeed manifests phenomena known for the complex analytic maps, like Mandelbrot and Julia sets, at least on the visible coarse scale level. Moreover, it takes place in a wider parameter range than one could expect from the point of view of applicability of the shortened amplitude equations. Does this similarity spread out onto small-scale fractal structure of the sets? It appears that this is not the case. Responsible for this is violation of the complex analyticity.

Given an iterative complex analytic map $z_{n+1} = f(z_n)$, $z = X + iY$, one can separate real and imaginary parts in the equation and arrive at equivalent description of the dynamics by a real two-dimensional map

$$X_{n+1} = U(X_n, Y_n), \qquad Y_{n+1} = V(X_n, Y_n), \tag{40}$$

where $f(z) = U(X, Y) + iV(X, Y)$. This is a map of a special kind because the functions must satisfy to the Cauchy -Riemann equations

$$\frac{\partial U(X,Y)}{\partial X} = \frac{\partial V(X,Y)}{\partial Y}, \qquad \frac{\partial V(X,Y)}{\partial X} = -\frac{\partial U(X,Y)}{\partial Y}, \tag{41}$$

which imply vanishing of a derivative of the function f over the complex conjugate variable:

$$\frac{\partial f}{\partial z^*} = \left(\frac{\partial U}{\partial X} - \frac{\partial V}{\partial Y}\right) + i\left(\frac{\partial U}{\partial Y} + \frac{\partial V}{\partial X}\right) = 0. \tag{42}$$

[1]We avoid the term 'Mandelbrot set' because factual small-scale structure of these objects may be (and is, naturally, see below) distinct from that of fractal nature in the convenient Mandelbrot set.

As known, even a small smooth variation of the functions U and V violating the condition of complex analyticity implies generically radical changes in the dynamics, e.g. destruction of the small-scale fractal structure of the Mandelbrot set and of intrinsic universal scaling regularities [17, 18, 19, 20].

Let us look at the complex amplitude equations (6), which are equivalent to the original equations formulated in real variables. Observe that they contain some terms proportional to complex conjugate amplitudes A^* and B^*. These terms are oscillating, and they disappear under averaging procedure leading to the shortened amplitude equations (7). Nevertheless, the Poincaré map constructed from the precise equation (6) inevitably will contain the dependences of the conjugate variables violating the Cauchy - Riemann conditions. This violation may be as small as desired in the asymptotic of large N. At relatively small N, the effect of destruction of the small-scale structure of the Mandelbrot set becomes observable in computations.

One tool for analysis of degree of violation of the complex analyticity is computation of a spectrum of Lyapunov exponents. In particular, for a two-dimensional map $X_{n+1} = U(X_n, Y_n)$, $Y_{n+1} = V(X_n, Y_n)$ they may be determined via eigenvalues of the matrix

$$\mathbf{b} = \mathbf{a}(X_0, Y_0)\mathbf{a}^+(X_0, Y_0)\mathbf{a}(X_1, Y_1)\mathbf{a}^+(X_1, Y_1)...\mathbf{a}(X_{M-1}, Y_{M-1})\mathbf{a}^+(X_{M-1}, Y_{M-1}), \tag{43}$$

where

$$\mathbf{a} = \begin{pmatrix} \partial U(X,Y)/\partial X & \partial U(X,Y)/\partial Y \\ \partial V(X,Y)/\partial X & \partial V(X,Y)/\partial Y \end{pmatrix}, \tag{44}$$

In the case of a two-dimensional real map equivalent to an analytic map of one complex variable, two Lyapunov exponents must be equal. It may be shown from the Cauchy - Riemann conditions that two eigenvalues coincide at any values of parameters and variables. The same is true for the Lyapunov exponents expressed as $\Lambda_{1,2} \cong \log \lambda_{1,2}/2M$.

The non-autonomous system (2) possesses four Lyapunov exponents (we exclude the perturbations associated with a shift along the trajectory, or with a phase of the external driving, as it is commonly used in concern of the periodically non-autonomous systems). To compute the Lyapunov exponents we used the Benettin algorithm [21]. The procedure consists in simultaneous numerical solution of the equations (2) and a collection of four exemplars of the linearized equations for small perturbations:

$$\begin{array}{l} \ddot{\widetilde{x}} + \omega_0^2 \widetilde{x} + F \cdot (\gamma + \sin \Omega t)\dot{\widetilde{x}} = \varepsilon \widetilde{y} \sin \omega_0 t, \\ \ddot{\widetilde{y}} + (2\omega_0)^2 \widetilde{y} + F \cdot (\gamma - \sin \Omega t)\dot{\widetilde{y}} = 2\varepsilon x \widetilde{x}. \end{array} \tag{45}$$

At each period $T = 2\pi/\Omega$ we perform Gram-Schmidt orthogonalization and normalization for a set of four vectors $\widetilde{\mathbf{x}}^j = \{\widetilde{x}^j, \dot{\widetilde{x}}^j/\omega_0, \widetilde{y}^j, \dot{\widetilde{y}}^j/2\omega_0\}$, $j = 1, ..., 4$. The Lyapunov exponents are estimated as mean rates of growth or decrease of logarithms of the norms of these four vectors:

$$\Lambda_j = \frac{1}{MT} \sum_{i=1}^{M} \ln \|\widetilde{\mathbf{x}}_i^j\|, \qquad j = 1, ..., 4, \tag{46}$$

where the norms are evaluated after the orthogonalization but before the normalization.

In accordance to the computations, two larger exponents in dependence on the regime may be negative (periodic attractive orbits), positive (chaotic motions) and zero (a border of chaos and quasiperiodic regimes). The rest two exponents are always negative in the whole domain

of existence of bounded dynamical states (i.e. on the Mandelbrot set). In the left column of Fig. 6 we present charts of the largest Lyapunov exponent on the plane $(\lambda \sin\varphi, \lambda\cos\varphi)$ for three values of N. Gray tones from light to dark correspond to variation of the Lyapunov exponent from 0 to $-\infty$. The diagram on panel (a) corresponds to $N = 10$. Observe that at central parts of the leaves the largest Lyapunov exponent becomes large negative, which corresponds to periodic motions of high stability. At edges of the leaves, a thin strip of appearance of positive Lyapunov exponent takes place (chaos). The picture visually is similar to that for the map (1); see e.g. Ref. [17]. With decrease of N (Fig. 6, c), distortion of the configuration develops. The leaves lose a round form; wider strip of chaos and quasiperiodicity appears. In the right column of Fig. 6, we depict respective charts for a difference of two larger Lyapunov exponents. In the top diagram this difference does not exceed 10^{-2} that is comparable with numerical errors. However, at smaller N (panels e, f) regions of large difference of the exponent appear (black color). It reveals essential deflection from the complex analytic dynamics.

The equality for a pair of larger Lyapunov exponent should be regarded rather as an indirect symptom of the complex analytic dynamics. Let us turn to computations intended to straightforward verification of the Cauchy - Riemann equations (41). In application to the four-dimensional Poincaré map

$$\mathbf{x}_{n+1} = \mathbf{F}(\mathbf{x}_n), \tag{47}$$

where $\mathbf{x}$ is a vector $\{x, u, y, v\} = \{x, \dot{x}/\omega_0, y, \dot{y}/2\omega_0\}$, we produce the following procedure. In the course of dynamics of the system on several periods of modulation, we perform numerical solution of the equations (2) and of the set of equations for four perturbation vectors (45) with redefinition of them at the beginning of each period in accordance with

$$\begin{array}{l} \widetilde{\mathbf{x}}^1(nT+0) = \{\widetilde{x}, 0, 0, 0\}, \\ \widetilde{\mathbf{x}}^2(nT+0) = \{0, \widetilde{u}, 0, 0\}, \\ \widetilde{\mathbf{x}}^3(nT+0) = \{0, 0, \widetilde{y}, 0\}, \\ \widetilde{\mathbf{x}}^4(nT+0) = \{0, 0, 0, \widetilde{v}\}. \end{array} \tag{48}$$

At the end of each period, we compose a matrix

$$\mathbf{A} = \begin{pmatrix} \widetilde{\mathbf{x}}^{11}(nT-0)/\widetilde{x} & \widetilde{\mathbf{x}}^{21}(nT-0)/\widetilde{u} & \widetilde{\mathbf{x}}^{31}(nT-0)/\widetilde{y} & \widetilde{\mathbf{x}}^{41}(nT-0)/\widetilde{v} \\ \widetilde{\mathbf{x}}^{12}(nT-0)/\widetilde{x} & \widetilde{\mathbf{x}}^{22}(nT-0)/\widetilde{u} & \widetilde{\mathbf{x}}^{32}(nT-0)/\widetilde{y} & \widetilde{\mathbf{x}}^{42}(nT-0)/\widetilde{v} \\ \widetilde{\mathbf{x}}^{13}(nT-0)/\widetilde{x} & \widetilde{\mathbf{x}}^{23}(nT-0)/\widetilde{u} & \widetilde{\mathbf{x}}^{33}(nT-0)/\widetilde{y} & \widetilde{\mathbf{x}}^{43}(nT-0)/\widetilde{v} \\ \widetilde{\mathbf{x}}^{14}(nT-0)/\widetilde{x} & \widetilde{\mathbf{x}}^{24}(nT-0)/\widetilde{u} & \widetilde{\mathbf{x}}^{34}(nT-0)/\widetilde{y} & \widetilde{\mathbf{x}}^{44}(nT-0)/\widetilde{v} \end{pmatrix}. \tag{49}$$

In the case of exact fulfillment of the conditions of analyticity of the map (47) the elements must satisfy

$$\begin{array}{llll} \mathbf{A}^{11} = \mathbf{A}^{22}, & \mathbf{A}^{12} = -\mathbf{A}^{21}, & \mathbf{A}^{31} = \mathbf{A}^{42}, & \mathbf{A}^{32} = -\mathbf{A}^{41}, \\ \mathbf{A}^{13} = \mathbf{A}^{24}, & \mathbf{A}^{14} = -\mathbf{A}^{23}, & \mathbf{A}^{33} = \mathbf{A}^{44}, & \mathbf{A}^{43} = -\mathbf{A}^{34}. \end{array} \tag{50}$$

Alternatively, it is convenient to consider derivatives of the complex functions F_1 and F_2, defined as components of the vector function (47) over the conjugate variables $p^* = x - iu$ and $q^* = y - iv$, from which one can diagnose presence or absence of the non-analyticity:

$$\begin{array}{ll} \frac{\partial F_1}{\partial p^*} = (\mathbf{A}^{11} - \mathbf{A}^{22}) + i(\mathbf{A}^{12} + \mathbf{A}^{21}), & \frac{\partial F_1}{\partial q^*} = (\mathbf{A}^{31} - \mathbf{A}^{42}) + i(\mathbf{A}^{32} + \mathbf{A}^{41}), \\ \frac{\partial F_2}{\partial p^*} = (\mathbf{A}^{13} - \mathbf{A}^{24}) + i(\mathbf{A}^{14} + \mathbf{A}^{23}), & \frac{\partial F_2}{\partial q^*} = (\mathbf{A}^{33} - \mathbf{A}^{44}) + i(\mathbf{A}^{43} + \mathbf{A}^{34}). \end{array} \tag{51}$$

In Fig. 7 we present a plot for logarithm of absolute value of the derivative $|\partial F_1/\partial p^*|$ at the origin ($\mathbf{x}(0) = (0,0,0,0)$) with $\lambda = 0$ versus the parameter N , that is the dimensionless period of modulation. This is a quantifier or a degree of non-analyticity of the function under consideration. The data are approximated by a straight line with slope -1.86. It means that the degree of non-analyticity determined at the origin manifests exponential decay with growth of N as $F_1(p, p^*, q, q^*) \sim e^{-1.86}p^*$.

Figure 8 presents diagrams illustrating distribution of the maximal values of ratios

$$\begin{array}{cc} d_1 = \left|\frac{\partial F_1}{\partial p^*}\right| \Big/ \left|\frac{\partial F_1}{\partial p}\right|, & d_2 = \left|\frac{\partial F_1}{\partial q^*}\right| \Big/ \left|\frac{\partial F_1}{\partial q}\right|, \\ d_3 = \left|\frac{\partial F_2}{\partial p^*}\right| \Big/ \left|\frac{\partial F_2}{\partial p}\right|, & d_4 = \left|\frac{\partial F_2}{\partial q^*}\right| \Big/ \left|\frac{\partial F_2}{\partial q}\right| \end{array} \tag{52}$$

on the parameter plane $\lambda e^{i\varphi}$. The values are determined along the orbits starting from the origin of length equal to 100 modulation periods. Gray scales from light to dark correspond to growth of d, i.e. to increase of degree of deflection of the dynamics from the pure complex analytical. Observe that at small N (panel c), wide regions of essential violation of the Cauchy - Riemann conditions take place, where the ratios of derivatives in respect to complex variable and the conjugate variable exceed 1. For larger N, when the cactuses look yet similar to the Mandelbrot set (panels a and b), analogous violations occur only on the small-scale details of the Mandelbrot-like structure (see Fig. 9).

It is interesting to evaluate degree of violation of the analyticity globally in the phase space of the system or, at least, in domains including the basins of attraction. In Fig. 10 we present data of computations aimed to estimate maximal absolute value for the derivative ratios (52) on the plane (x, u). Observe that with decrease of the parameter N the picture becomes darker (the color coding is assumed the same as in Fig. 8, a-c). In Fig. 11 we present plots for maximal values of d_i ($i = 1, ..., 4$) determined in a domain of a four-dimensional cube in the phase space containing the attraction basins. (Computations were produced at nodes of four-dimensional grid of size $50 \times 50 \times 50 \times 50$.) Observe that at small N the derivatives over the conjugate variables become rather large in comparison with derivatives in respect to the main complex variable; for N <4 they may be larger even by many times.

As follows from our computations, the system of coupled non-autonomous oscillators indeed demonstrates dynamics roughly corresponding to that in the complex analytic map. Degree of the correspondence is determined by parameter N, that is a ratio of modulation period to period of basic oscillations. With decrease of N, the type of dynamics is changed gradually; the destruction of the picture associated with the complex analytic dynamics starts from small-scale details of the visible structure of the Mandelbrot set.

5 Conclusion

In this paper, a system was proposed that consists of two coupled alternately excited oscillators with a turn-by-turn transfer of the excitation from one to another, accompanied with appropriate nonlinear transformation of the complex amplitude of the oscillations in the course of the process. This system obviously allows realization as a physical object, e.g. as an electronic devise analogous to that described in Ref. [10]. Analytic consideration showed that the Poincaré map for the system corresponds in a definite approximation to a complex quadratic map. Numerical studies confirm

presence of the expected phenomena intrinsic to iterative complex analytic maps (like Mandelbrot set, Julia sets etc.) at least up to a definite level of resolution of the fractal-like structures. Analysis of violation of the applicability of the approximation corresponding to the complex quadratic map revealed several effects. One is rotation of the Mandelbrot-like set in the complex parameter plane, and other is destruction of the small-scale fractal structure under decrease of the parameter representing a ratio of the modulation period to the period of basic oscillations.

Acknowledgement

The work is performed under partial support of RFBR (Grant No 06-02-16619). O.B.I. acknowledges support from INTAS (Grant 05-109-5262) and from Grant of the President of Russian Federation (MK-8501.2006.2).

References

[1] H.-O. Peitgen and P.H. Richter, The beauty of fractals. Images of complex dynamical systems, Springer-Verlag, New-York, 1986.

[2] H.-O. Peitgen, H. Jurgens, and D. Saup, Chaos and fractals: new frontiers of science, Springer-Verlag, New-York, 1992.

[3] R.L. Devaney, An Introduction to chaotic dynamical systems, Addison-Wesley, New York, 1989.

[4] C. Beck, Physical meaning for Mandelbrot and Julia set, Physica D125 (1999) 171-182.

[5] O.B. Isaeva, On possibility of realization of the phenomena of complex analytical dynamics for the physical systems built up of coupled elements, which demonstrate period-doublings, Applied Nonlinear Dynamics (Saratov) 9 (6) (2001) 129-146 (in Russian).

[6] O.B. Isaeva and S.P. Kuznetsov, On possibility of realization of the phenomena of complex analytic dynamics in physical systems. Novel mechanism of the synchronization loss in coupled period-doubling systems, Preprint http://xxx.lanl.gov/abs/nlin.CD/0509012.

[7] O.B. Isaeva and S.P. Kuznetsov, On possibility of realization of the Mandelbrot set in coupled continuous systems, Preprint http://xxx.lanl.gov/abs/nlin.CD/0509013.

[8] O.B. Isaeva, S.P. Kuznetsov, and V.I. Ponomarenko, Mandelbrot set in coupled logistic maps and in an electronic experiment, Phys. Rev. E64 (2001) 055201(R).

[9] S.P. Kuznetsov, Example of a physical system with a hyperbolic attractor of the Smale-Williams type, Phys. Rev. Lett. 95 (2005) 144101.

[10] S.P. Kuznetsov and E.P. Seleznev, Strange attractor of Smale-Williams type in the chaotic dynamics of a physical system, J. of Exp. and Theor. Phys. 102 (2) (2006) 355-364.

[11] S.P. Kuznetsov and I.R. Sataev, Hyperbolic attractor in a system of coupled non-autonomous van der Pole oscillators: Numerical test for expanding and contracting cones, Phys. Lett. A (2007) (in press).

[12] O.B. Isaeva, A.Yu. Jalnine and S.P. Kuznetsov, Arnold's cat map dynamics in a system of coupled non-autonomous van der Pol oscillators, Phys. Rev. E74 (2006) 046207.

[13] A.Yu. Zhalnin and S.P. Kuznetsov, On the realization of the Hunt-Ott strange nonchaotic attractor in a physical system, J. Technical Physics 52 (4) (2007) 401-408.

[14] O.B. Isaeva and S.P. Kuznetsov, Period tripling accumulation point for complexified Hénon map, Preprint http://xxx.lanl.gov/abs/nlin.CD/0509015.

[15] J.H. Hubbard and R.W. Oberste-Vorth, Hénon mappings in the complex domain: Projective and inductive limits of polynomials, Preprint http://www.math.sunysb.edu/preprints.html.

[16] O. Biham, W. Wenzel, Unstable periodic orbits and the symbolic dynamics of the complex Hénon map, Phys. Rev. A42 (8) (1990) 4639-4646.

[17] O.B. Isaeva and S.P. Kuznetsov, On scaling properties of two-dimensional maps near the accumulation point of the period-tripling cascade, Regular and Chaotic Dynamics 5 (4) (2000) 459-476.

[18] B.B. Peckham, Real perturbation of complex analytic families: Points to regions, Int. J. of Bifurcation and Chaos 8 (1998) 73-94.

[19] B.B. Peckham, Real continuation from the complex quadratic family: Fixed-point bifurcation sets, Int. J. of Bifurcation and Chaos 10 (2) (2000) 391-414.

[20] J. Argyris, I. Andreadis and T.E. Karakasidis, On perturbations of the Maldelbrot map, Chaos, Solitons & Fractals 11 (7) (2000) 2067-2073.

[21] G. Benettin, L. Galgani, A. Giorgilli and J.-M. Strelcyn, Lyapunov characteristic exponents for smooth dynamical systems and for Hamiltonian systems: A method for computing all of them. Part I: Theory. Part II: Numerical application, Meccanica 15 (1980) 9-30.

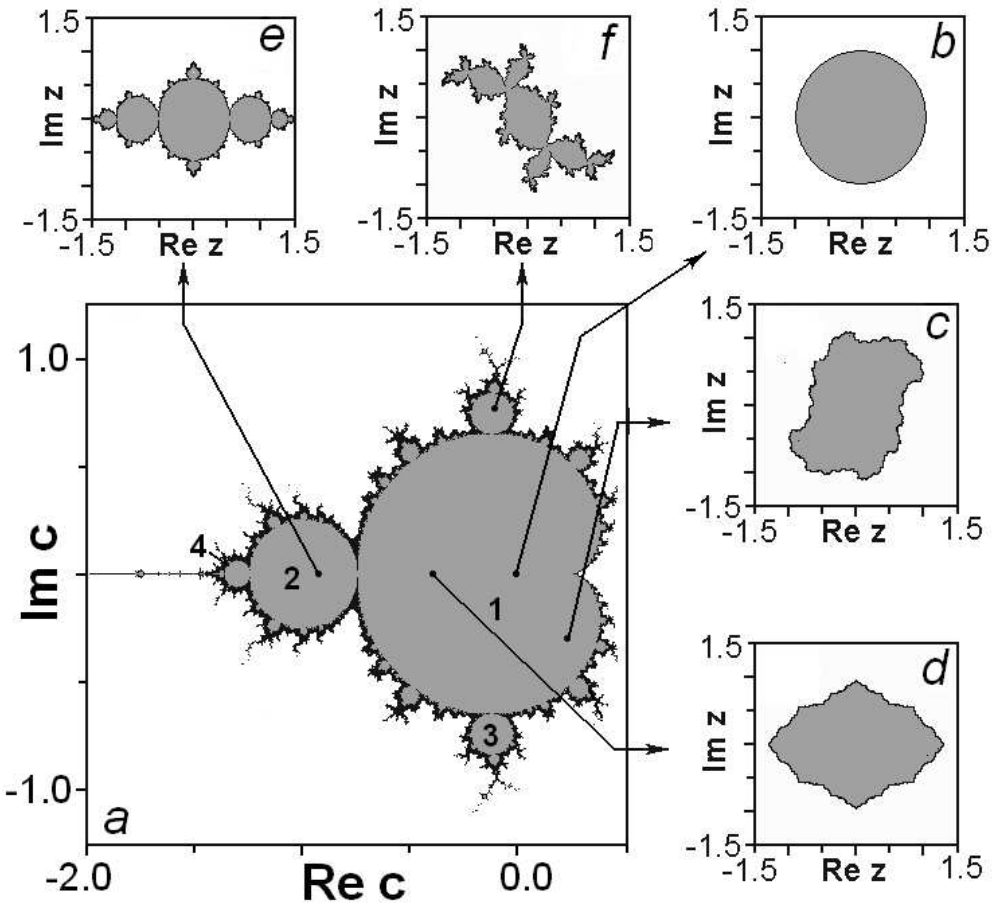

Figure 1: Mandelbrot set (a) and Julia sets for the complex quadratic map (1) at several values of the parameter $c = 0.0$ (b), $c = 0.2-0.3i$ (c), $c = -0.4$ (d), $c = -0.8$ (e), $c = -0.1+0.75i$ (f). Gray areas correspond to periodic dynamics in a bonded domain of the complex variable z (the periods are marked by figures). Black designates bounded chaotic dynamics, and white corresponds to escape of the iterations to infinity.

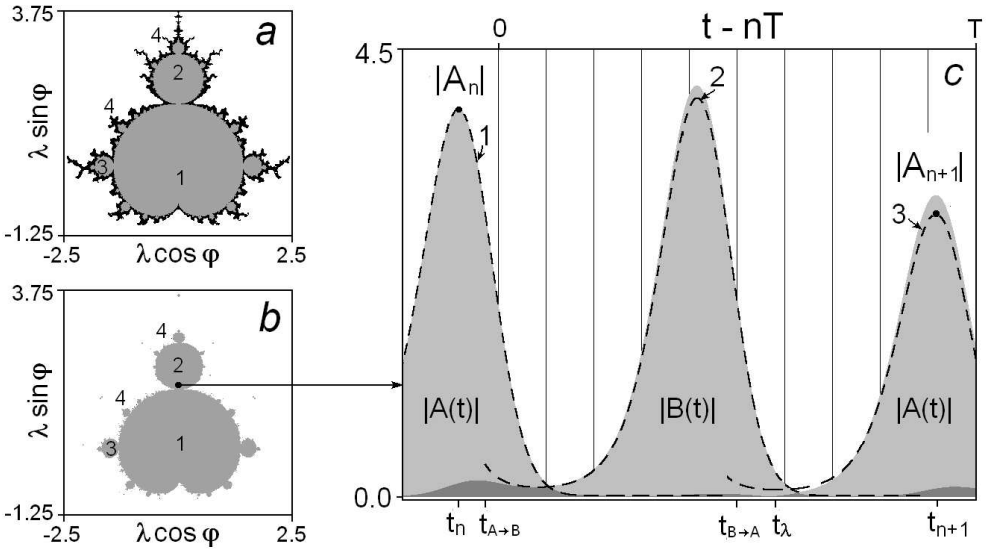

Figure 2: Mandelbrot set for the map (37) (a) and domains of observable bounded periodic dynamics (gray) in a system of shortened amplitude equations (7) (b) at parameter values $F = 7$, $\gamma = 0.5$, $\omega_0 = 2\pi$, $N = 10$, $\varepsilon = 1$. Amplitudes of two oscillators versus time are shown in panel (c) at $\lambda = 1.5i$. Gray profiles correspond to numerical solution of the equations (7), and dotted lines (1-3) designate the approximate analytic solution in accordance with (15) (1), (23) (2), (36) (3).

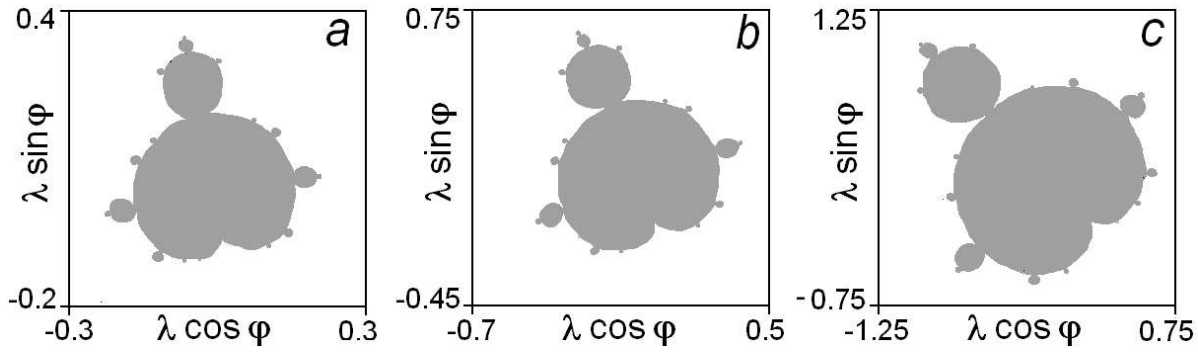

Figure 3: Mandelbrot cactuses for the system of coupled non-autonomous oscillators (2) (or for equivalent amplitude equations (6)). Parameter values: (a) $N = 80$, $F = 0.875$, $\varepsilon = 0.125$, (b) $N = 40$, $F = 1.75$, $\varepsilon = 0.25$, and (c) $N = 20$, $F = 3.5$, $\varepsilon = 0.5$. For all cases, $\omega_0 = 2\pi$ and $\gamma = 0.5$. Compare with the portrait in Fig. 2 b corresponding to the large-N asymptotic and observe visible counter-clock-wise rotation of the cactuses under decrease of N.

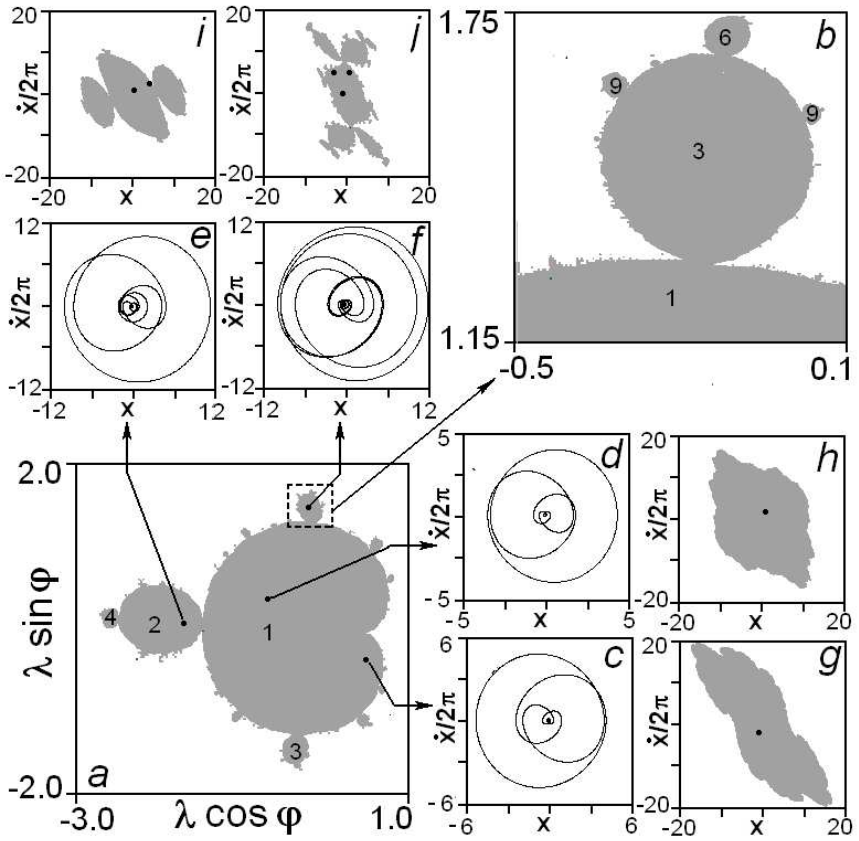

Figure 4: The Mandelbrot cactus (a) and its magnified fragment (b) for the system of coupled non-autonomous oscillators (2) at $\omega_0 = 2\pi$, $F = 7$, $\gamma = 0.5$, $N = 10$, $\varepsilon = 1$ on the plane of a complex parameter $\lambda e^{i\varphi}$. Gray color corresponds to presence of attractive periodic orbits. The figures 1, 2, 3... designate the period in units of the basic modulation period $T = 2\pi/\Omega$. White color corresponds to absence of attractive periodic motions and escape to infinity. For the parameter values marked with dots (panel a), portraits of the attractive periodic orbits are shown in projection on the plane $(x, \dot{x}/2\pi)$ (panels c and f) together with cross-sections of the basins of attraction for these orbits with this coordinate plane (g and j). Dots inside the basins correspond to the stroboscopic cross-sections for those periodic orbits. The panels correspond to the parameter sets: $\lambda\cos\varphi = 0.5$, $\lambda\sin\varphi = -0.2$ (c and g), $\lambda\cos\varphi = -0.7$, $\lambda\sin\varphi = 0.4$ (d and h), $\lambda\cos\varphi = -1.7$, $\lambda\sin\varphi = 0.1$ (e and I), $\lambda\cos\varphi = -0.2$, $\lambda\sin\varphi = 1.5$ (f and j).

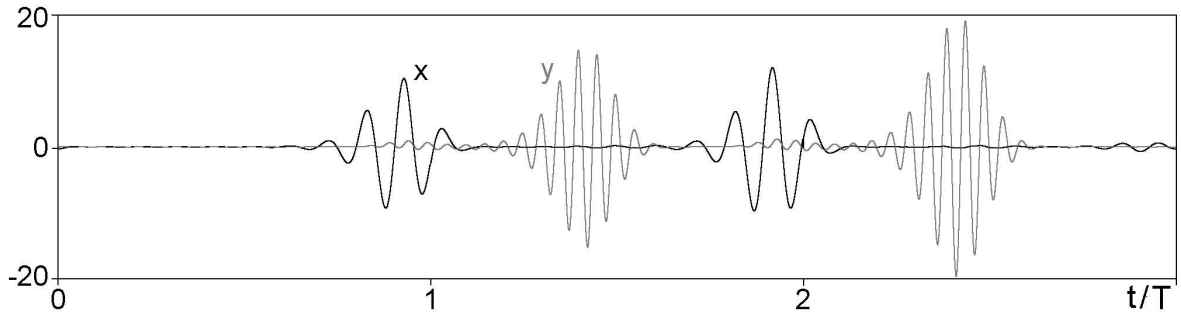

Figure 5: Dynamical variables versus time for the system of coupled non-autonomous oscillators (2) at $\omega_0 = 2\pi$, $F = 7$, $\gamma = 0.5$, $\varepsilon = 1$, $N = 10$, $\lambda e^{i\varphi} = -0.2 + 1.5i$ that corresponds to presence of an attractive cycle of period 3 in the Poincaré map. (The shown pattern is repeated again and again with period $3T$.)

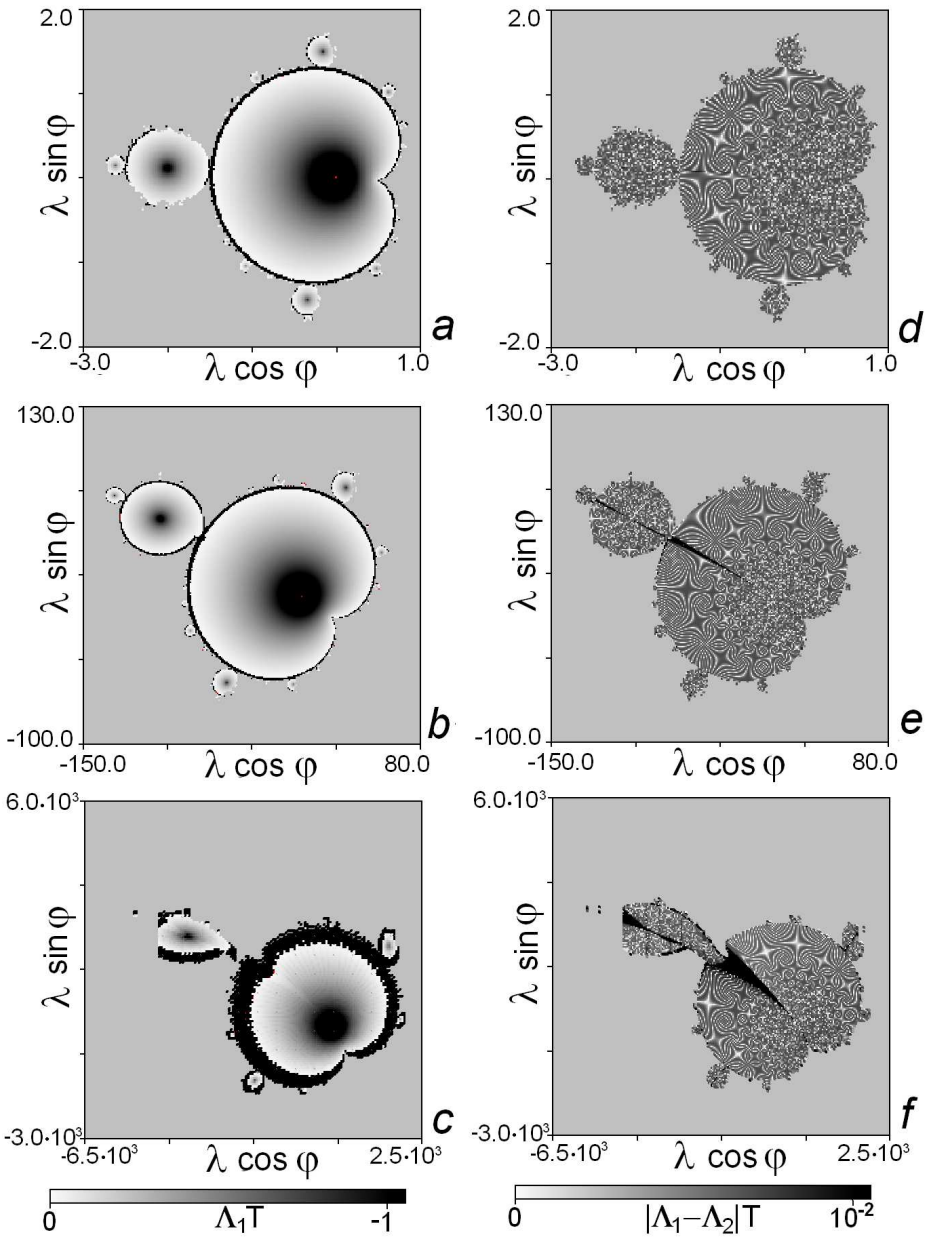

Figure 6: Charts of the largest Lyapunov exponent (*a*-*c*) and diagrams for a difference of two larger exponents (*d*-*f*) for the system of coupled non-autonomous oscillators (2) at three values of the ratio of periods of modulation and of basic oscillators: $N = 10$ (*a*, *d*), 6 (*b*, *e*), 3 (*c*, *f*). Other parameters: $\omega_0 = 2\pi$, $F = 7$, $\gamma = 0.5$, $\varepsilon = 1$. Uniform gray color means area of unstable dynamics (typically divergence to infinity). Legend for gray scales is shown at the bottom for both two columns. Black color on the diagrams in the left column also corresponds to chaotic dynamics in a bounded domain.

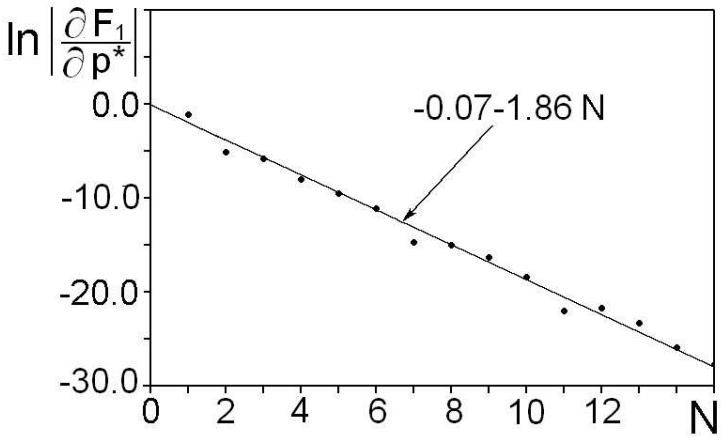

Figure 7: Logarithm of absolute value of derivative for one of the functions determining the two-dimensional complex Poincaré map $p_{n+1} = F_1(p_n, q_n)$, $q_{n+1} = F_2(p_n, q_n)$ over the complex conjugate variable. The complex variables are expressed via real physical variables of the system (2) as $p = x + i\dot{x}/\omega_0$, $q = y + i\dot{y}/2\omega_0$. The derivative was evaluated at the origin $x = 0$, $\dot{x} = 0$, $y = 0$, $\dot{y} = 0$ for $\lambda = 0$. Other parameters are $\omega_0 = 2\pi$, $F = 7$, $\gamma = 0.5$, $\varepsilon = 1$.

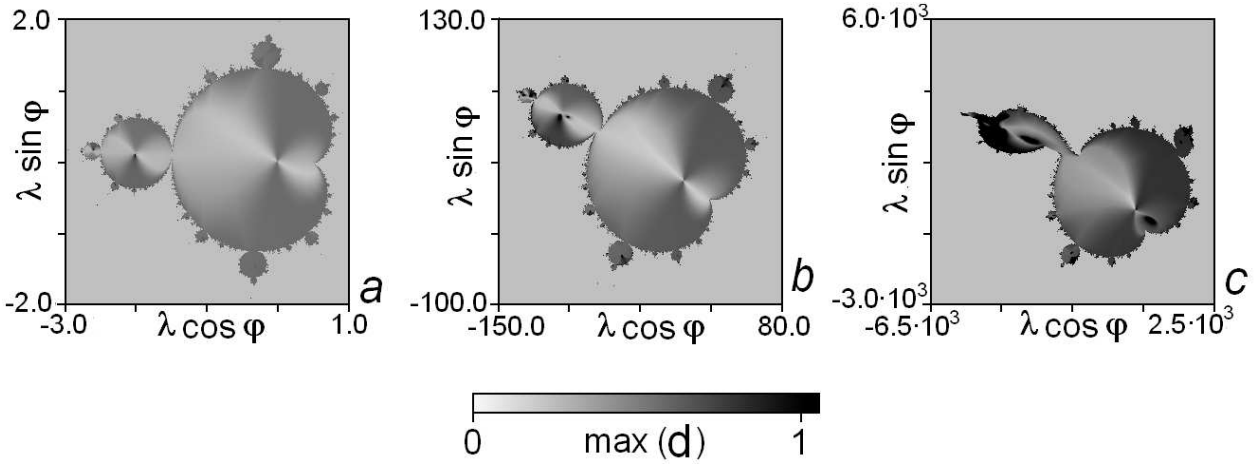

Figure 8: Distributions of the maximal ratios for derivatives (49) over the plane of complex parameter $\lambda e^{i\varphi}$. The values are determined along the orbits starting from the origin, of length equal to 100 modulation periods. Gray scales from light to dark correspond to increase of degree of deflection of the dynamics from the pure complex analytical. The diagrams are drown for N = 10 (a), 6 (b), 3 (c). Other parameters are the same as in Fig. 4.

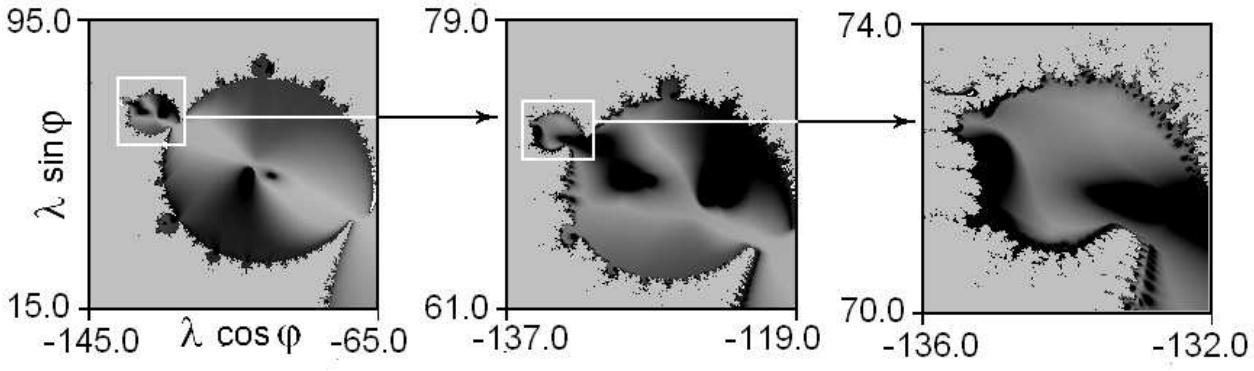

Figure 9: Magnified fragments of Fig. 8, *b*.

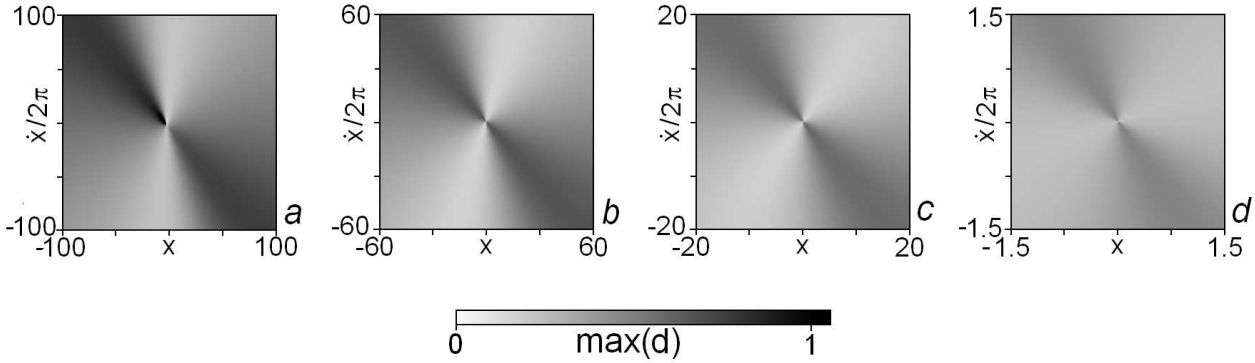

Figure 10: Distributions of the maximal ratios for derivatives (49) over the plane of complex parameter $\lambda e^{i\varphi}$ determined for one modulation period. The diagrams are drown for $N = 3$ (a), 6 (b), 10 (c) , 15 (d). Other parameters are $\lambda = 0$, $\omega_0 = 2\pi$, $F = 7$, $\gamma = 0.5$, $\varepsilon = 1$.

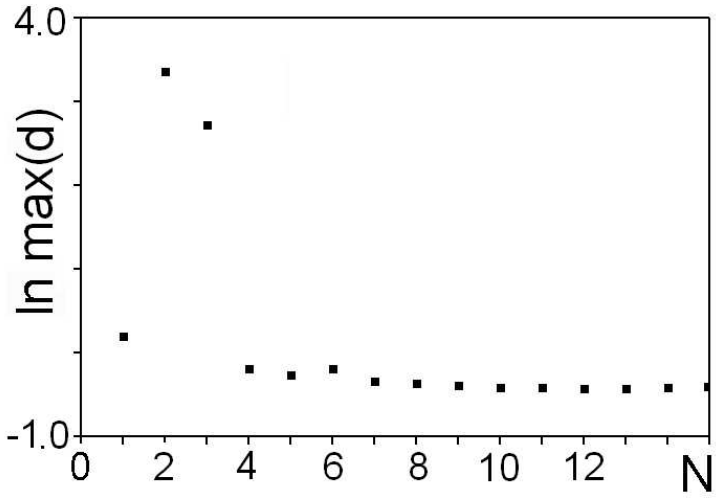

Figure 11: Logarithm of the maximal value of the ratios of derivatives d computed on one iteration of the Poincaré map over nodes of array of size $50 \times 50 \times 50 \times 50$ on a domain of a four-dimensional cube in the phase space containing the basins of attraction. The diagram is drawn for $\lambda = 0$, $\omega_0 = 2\pi$, $F = 7$, $\gamma = 0.5$, $\varepsilon = 1$.